Monthly Notices
of the
ROYAL ASTRONOMICAL SOCIETY

Mon. Not. R. Astron. Soc. **423,** 1825–1830 (2012) doi:10.1111/j.1365-2966.2012.21006.x

# Ly$\alpha$-induced charge effects of polycyclic aromatic hydrocarbons embedded in ammonia and ammonia:water ice

Steven H. Cuylle,[1] Emily D. Tenenbaum,[1] Jordy Bouwman,[1] Harold Linnartz[1]⋆ and Louis J. Allamandola[2]

[1]*Raymond and Beverly Sackler Laboratory for Astrophysics, Leiden Observatory, Leiden University, PO Box 9513, NL 2300 RA Leiden, the Netherlands*
[2]*NASA Ames Research Center, Space Science Division, Mail Stop 245-6, Moffett Field, CA 94035, USA*

Accepted 2012 March 27. Received 2012 March 27; in original form 2012 February 3

**ABSTRACT**

Infrared emission features assigned to gas phase polycyclic aromatic hydrocarbons (PAHs) are observed in space along many lines of sight. In regions where interstellar ices are present, these emissions are largely quenched. It is here that PAHs form agglomerates covered by ice or freeze out on to dust grains, together with volatile species such as $H_2O$, CO, $CO_2$ and $NH_3$. Upon exposure to the Ly$\alpha$-dominated interstellar radiation field, PAHs are expected to participate in photo-induced chemical reactions, explicitly also involving the surrounding ice matrix.

In this paper, a systematic laboratory-based study is presented for the solid-state behaviour of the PAHs pyrene and benzo[ghi]perylene upon Ly$\alpha$ irradiation in ammonia and mixed $NH_3$:$H_2O$ astronomical ice analogues. The results are compared to recently published work focusing on a pure water ice environment. It is found that the ice matrix acts as an 'electronic solid-state switch' in which the relative amount of water and ammonia determines whether positively or negatively charged PAHs form. In pure water ice, cations are generated through direct ionization, whereas in pure ammonia ice, anions form through electron donation from ammonia-related photoproducts. The solid-state process controlling this latter channel involves electron transfer, rather than acid–base type proton transfer. In the mixed ice, the resulting products depend on the mixing ratio. The astronomical consequences of these laboratory findings are discussed.

**Key words:** astrochemistry – molecular processes – methods: laboratory – ISM: molecules.

## 1 INTRODUCTION

The astrospectroscopic identification of individual polycyclic aromatic hydrocarbons (PAHs) has not yet been realized. Microwave spectra of gas phase PAHs are not available because they have, at best, weak permanent dipole moments. The transitions in those that do have permanent dipoles – arising from isotope or hetero-atom substitutions – suffer from severe band dilution due to the high partition function. The presence of PAHs in space, however, is generally accepted because of the observation of a set of strong infrared (IR) emission lines around 3.3, 6.2, 7.7, 8.6 and 11.2 μm that have been explained by PAH emission following ultraviolet (UV) excitation (Tielens 2008, and references therein). PAH mid-IR emissions are observed along many lines of sight: molecular cloud edges, photodissociation regions, planetary nebulae and even in other galaxies, with the exception of dense clouds, where these features are quenched. Here, volatile molecules freeze out, forming layers of ice on small dust grains (Pontoppidan, van Dishoeck & Dartois 2004; Öberg et al. 2010), providing a solid-state molecule reservoir. Subsequently, chemical triggers – photon irradiation and particle bombardment – drive solid-state reactions that have been shown in the laboratory to provide pathways towards molecular complexity in space (Fuchs et al. 2009; Öberg et al. 2009; Linnartz et al. 2011, and references therein). Less volatile species, such as PAHs are also expected to condense under these conditions. This effectively quenches the emission process upon UV excitation and explains the missing mid-IR emission features in dense clouds. Indeed, in young stellar objects (YSOs), observations indicate that PAHs likely exist in the solid phase, either as components of ice mantles or as PAH conglomerates (Geers et al. 2009). Consequently, PAHs are also expected to participate in the solid-state chemical network that is responsible for the formation of larger organic compounds. Unfortunately, systematic laboratory studies focusing on this important process are largely lacking.

In situ spectroscopic studies of PAHs in ice environments comprise mainly of IR (Bernstein et al. 1999) and more recently optical work (Bouwman et al. 2009, 2010). Spectroscopic studies in the

⋆E-mail: linnartz@strw.leidenuniv.nl

optical and in the IR focusing on the UV-induced PAH chemistry have been reported specifically for PAHs embedded in water ice (Bernstein et al. 2007; Bouwman et al. 2011a,b; Guennoun, Aupetit & Mascetti 2011). Water is the most abundant constituent of interstellar ices and was shown in several recent studies to catalyse reactions (Öberg et al. 2010) and to promote cation formation (Bouwman et al. 2011b). In this work, we investigate to which extent a different matrix environment (pure ammonia or mixed with water) influences the ionization process. Ammonia was chosen since, after water, it is among the most abundant polyatomic interstellar molecules known. Past studies showed that ammonia is conducive to solid-state anion formation (Schutte & Khanna 2003). The study here is astronomically relevant, as mixed water:ammonia ice is widely present around YSOs (Bottinelli et al. 2010) and pure $NH_3$ ice has been found in planetary atmospheres such as that of Jupiter (Brooke et al. 1998; Baines, Carlson & Kamp 2002; Wong et al. 2004).

## 2 EXPERIMENTAL

The measurements are performed with OASIS, our Optical Absorption Setup for Ice Spectroscopy that monitors PAHs and PAH reaction products upon UV irradiation in situ and in real time. Experiments are performed on two commercially available PAH molecules: pyrene (Py, $C_{16}H_{10}$, Aldrich, 99 per cent) and benzo[ghi]perylene ($B_{ghi}P$, $C_{22}H_{12}$, Aldrich, 99 per cent). The experimental procedure applied here is the same as used in Bouwman et al. (2009, 2010, 2011b). Ices are grown on a cryogenically cooled $MgF_2$ sample (40 K) window that is located inside a high-vacuum chamber ($P < 5 \times 10^{-7}$ mbar) by flowing a gas mixture of PAH and pure ammonia (Praxair, 99.96 per cent, as commercially available) or mixed ammonia:water (milli-q, degassed with three freeze-pump-thaw cycles) from an external manifold. Pyrene vapour is created by heating solid pyrene inside a pyrex vial to ∼40° C. $B_{ghi}P$ has a much lower vapour pressure and PAH vapour is created by warming $B_{ghi}P$ powder in a resistively heated steel oven, affixed to the end of the gas deposition tube inside the vacuum chamber. In both cases, typical PAH:ice mixing ratios amount to approximately 1:5000.

During ice growth, the ice thickness is monitored via interference fringes resulting from the reflection of a HeNe laser beam off the sample window. Typical ice growth rates amount to 75 nm $min^{-1}$ and standard ices are calculated to be ∼1.3 μm thick, using an ammonia ice refractive index of 1.49 and a solid-state ammonia density of 0.86 g $cm^{-3}$ (Romanescu et al. 2010). After deposition, the ice is illuminated with vacuum UV photons produced by a microwave-powered hydrogen discharge lamp that emits not only Ly$\alpha$ photons (∼121.6 nm), but also a broader band around 160 nm (Caro et al. 2002). The emitted light is directed towards the ice substrate through a $MgF_2$ window that also acts as a vacuum seal. The lamp flux at the substrate surface is of the order of $10^{14}$–$10^{15}$ photons $cm^{-2}$ $s^{-1}$ (Bouwman et al. 2011b).

During an experiment, spectral properties are monitored in direct absorption, dispersing the light of an intense white light source (Xe-arc lamp) that is focused through the ice on to the slit of a broad-band ANDOR Shamrock spectrometer. This system disperses light in the 300–815 nm region with a maximum spectral resolution of 0.55 nm. Before the vacuum UV exposure starts, a reference spectrum is taken to which subsequent spectra are compared. Negative peaks then correspond to species being consumed, while positive peaks correspond to species newly formed. The spectra presented here are plotted in units of optical depth [OD = ln(I/$I_0$)]. Spectra are recorded for different ice temperatures between 12 and 80 K.

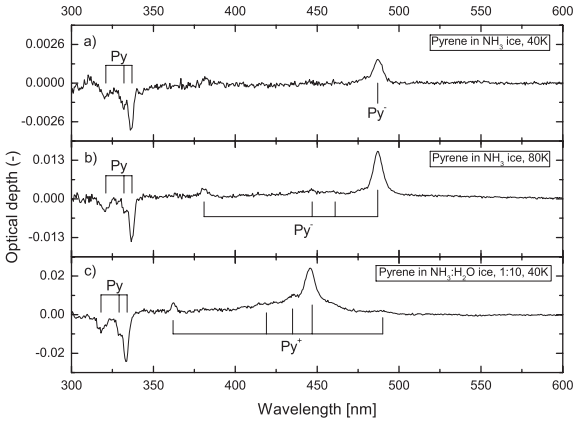


**Figure 1.** Spectra of pyrene ($C_{16}H_{10}$) containing ammonia ice (∼1:5000) acquired after 100 s of Ly$\alpha$ exposure. Negative peaks indicate the consumption of the precursor molecule and positive peaks indicate the formation of new species: (a) Pyrene in $NH_3$ ice at 40 K, (b) Pyrene in $NH_3$ ice at 80 K and (c) Pyrene in $NH_3$:$H_2O$ 1:10 ice at 40 K.

## 3 RESULTS

### 3.1 PAH:$NH_3$ Ly$\alpha$ photolysis

Fig. 1(a) shows a spectrum of Py:$NH_3$ (∼1:5000) ice at 40 K after 100 s of UV exposure. As was the case for Py in water ice (Bouwman et al. 2009), the negative absorption signal around 337 nm is due to Py consumption, but other spectral features clearly differ – both in wavelength and relative intensities – from the UV-irradiated Py water-dominated $NH_3$:$H_2O$ 1:10 ice spectrum (Fig. 1c). Immediately after photolysis starts, positive signals at 381 and 487 nm grow. These features can be assigned to the Py anion based on the work by Shida (1988). The identification is solidified by the same experiment conducted at 80 K (Fig. 1b), where the anion signal is more intense, also revealing weaker $Py^-$ features reported by Shida at 448 and 461 nm.

Remarkably, PAH anion production is favoured by the $NH_3$ ice, whereas PAH cation production is favoured by the $H_2O$ ice. To test if this is a general trend, the UV photolysis of another PAH, $B_{ghi}P$, in $NH_3$ ice has been studied. Spectral data from the $B_{ghi}P$ experiments are displayed in Fig. 2. Negative absorption bands at

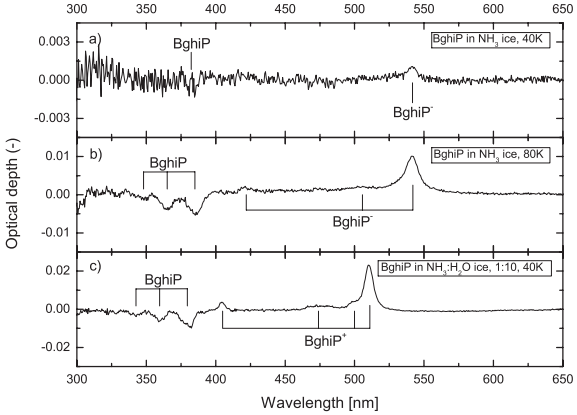


**Figure 2.** As Fig. 1 for benzo[ghi]perylene ($C_{22}H_{12}$).

**Table 1.** PAH transition wavelengths in $NH_3$ ice, $H_2O$ ice and in MTHF matrices, with the strongest transition first.

| Molecule | Transition | $\lambda_{peak}$ in $NH_3$ [a] (nm) | $\lambda_{peak}$ in $H_2O$ [b] (nm) | $\lambda_{peak}$ in MTHF [c] (nm) |
|---|---|---|---|---|
| Py | $S_2(^1B_{2u}) \leftarrow S_0(^1A_g)$ | 337.0 (5), 333.1 (5), 320.8 (5) | 334, 329, 319 | – |
| $Py^-$ | – | 486.9 (5), 381.4 (5), 448 (4), 461 (2) | – | 492, 383, 449, 463 |
| $B_{ghi}P$ | $S_2(^1B_2) \leftarrow S_0(^1A_1)$ | 384.7 (1.5), 366 (1) | 380, 360 | – |
| $B_{ghi}P^-$ | – | 541.2 (5), 419 (2), 505 (3) | – | 545, 423, 505 |

[a]In 80-K ice, uncertainties in parentheses.
[b]Bouwman et al. (2011b), in 25-K ice.
[c]Shida (1988), in 77-K 2-Methyltetrahydrofuran.

366 and 385 nm gradually grow, hard to see at 40 K (Fig. 2a), but clearly visible at 80 K (Fig. 2b), signalling consumption of neutral $B_{ghi}P$ ($^1B_2$). The latter is in correspondence with UV irradiation data found for $B_{ghi}P$ in a $NH_3$:$H_2O$ 1:10 ice (Fig. 2c), but again, the resulting reaction products differ from those in $H_2O$ ice. A positive band at 541 nm corresponds to the $B_{ghi}P$ anion (Shida 1988). As for Py, the 80-K experiment shows an improvement in signal-to-noise ratio and allows the detection of other anion bands at 419 and 505 nm as well. For both PAHs, Py and $B_{ghi}P$, the neutral PAH signal loss and PAH anion signal growth in ammonia ice are clearly weaker than the corresponding PAH cation signals in water ice.

The influence of ice temperature is further explored in experiments performed at 12, 40, 55 and 80 K. At higher temperatures, both PAH anion formation and PAH neutral consumption are more efficient. For example, at 80 K, after 100 s of Ly$\alpha$ exposure, the Py anion peak has an intensity of 0.014 OD units, while at 40 K the intensity is 10 times less. This is in contrast to water-based low-temperature ice chemistry where the cation formation is largest for lower temperatures (Bouwman et al. 2010).

In Table 1, the spectroscopic data for PAH (anions) in $NH_3$ ice are summarized. The observed wavelengths for the band maxima are compared to literature values of corresponding transitions in other matrix environments. Typically, the PAH anion wavelengths in $NH_3$ ice are a few up to ∼5 nm lower than in MTHF (2-methyltetrahydrofuran) glass at 77 K, and the PAH:$NH_3$ neutral peaks are 1.8–6 nm redshifted with respect to bands observed in a pure $H_2O$ ice.

### 3.2 PAH:$H_2O$/$NH_3$ UV photolysis

To compare the influence of a water or ammonia environment on the photochemistry in PAH containing ices, experiments have been performed on mixed $H_2O$:$NH_3$ ices. This is also a more realistic interstellar ice analogue, as in space (e.g. around YSOs) both water and ammonia are present in ices on cold dust grains, with typical $NH_3$ abundances with respect to $H_2O$ ranging from a few up to 15 per cent (Bottinelli et al. 2010). Laboratory measurements are performed for different mixing ratios that cover these astronomically relevant values. In addition to the experiments for PAHs in pure water and ammonia ices, experiments have been performed at 40 K for ices with $NH_3$:$H_2O$ mixing ratios of 100:1, 10:1, 5:1, 1:1 and 1:10. In all cases, the PAH:ice molecular ratio was kept at ∼1:5000. The measurements allow one to determine the transition region for which the cation-generating chemistry that dominates in pure water ice switches to anion-generating chemistry in pure ammonia ice. It is found that, as long as the water and ammonia amount are comparable, this switching point is not that well defined. The anion feature at 487 nm appears for samples with a $NH_3$:$H_2O$ fraction of 1:1 or higher and the cation feature at 445.6 nm is observed in ices with a 1:1 or higher $H_2O$:$NH_3$ fraction. In the 1:1 $NH_3$:$H_2O$ ice, both PAH anion and cation features are observed simultaneously as is illustrated in Fig. 3 for Py for irradiation times of 30 and 190 s. Nevertheless, the influence of the $NH_3$:$H_2O$ ratio of the ice on the relative amount of anion formation, Py:$Py^-$ is significant. Fig. 4 shows the anion feature at 487 nm, normalized with respect to the total Py abundance, at its maximum and for different ice compositions at 40 K. Compared to pure $NH_3$ ice (Fig. 4a), no

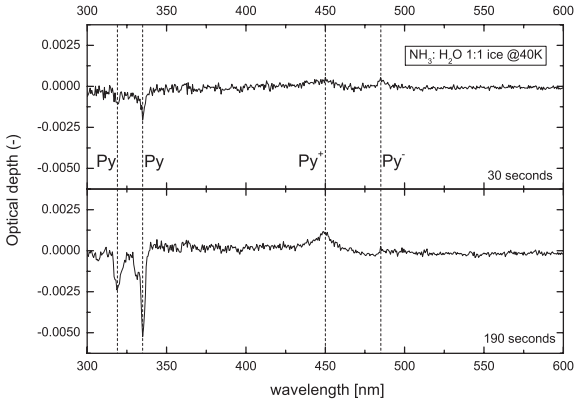


**Figure 3.** Spectra of pyrene in a $H_2O$:$NH_3$ 1:1 matrix at 40 K under vacuum UV photolysis (30 s in the upper panel and 190 s in the lower panel). Indicated are the wavelengths of the anion feature in $NH_3$ ice, the cation feature in $H_2O$ ice and the neutral features in $NH_3$ ice.

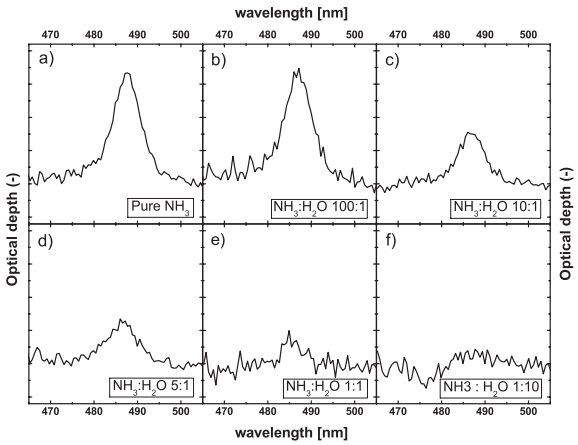


**Figure 4.** Maximum strength of the $Py^-$ feature for different ice compositions at 40 K, varying between pure ammonia and pure water ice: (a) $NH_3$, (b) $NH_3$:$H_2O$ 100:1, (c) $NH_3$:$H_2O$ 10:1, (d) $NH_3$:$H_2O$ 5:1, (e) $NH_3$:$H_2O$ 1:1 and (f) $NH_3$:$H_2O$ 1:10 (identical to $H_2O$).

significant difference is found in the 100:1 $NH_3$:$H_2O$ ice (Fig. 4b), as may be expected. When increasing the relative amount of water in the ice to 10:1 $NH_3$:$H_2O$ (Fig. 4c), the anion signal is halved. A further increase of the water fraction to 1:1 $NH_3$:$H_2O$ (Fig. 4e) goes along with a further reduction of the anion signal. For a 1:10 $NH_3$:$H_2O$ ice mixture (Fig. 4f), anion features are no longer observed. Instead, the spectrum is dominated by signals originating from PAH cations and is not distinguishable from a spectrum of a vacuum UV-irradiated PAH:$H_2O$ ice (without $NH_3$).

### 3.3 Reaction products

A characterization of the PAH reaction scheme in the ammonia and ammonia:water ice, similar to the scheme derived for pure water ice (Bouwman et al. 2010), is not straightforward, because the anion signals are not very strong and no other photoproduct bands are evident. A number of possible PAH reaction products, however, can be ruled out or, at least, are of limited importance, based on the non-detection of known spectral features in the studied wavelength region. For example, 1- and 2-aminopyrene have favourable electronic absorptions at 360 and 340 nm, respectively (Šoustek et al. 2008), neither of which are observed. This is an interesting result since amino-substituted coronene has been detected using very sensitive mass spectroscopic techniques in coronene:$NH_3$ ice irradiation experiments (Bernstein et al. 2002). This non-detection likely arises from the lower sensitivity of optical absorption spectroscopy. Another undetected species is monohydrogenated pyrene, which absorbs at 400 nm (Bouwman et al. 2010). Monodeprotonated pyrene (the pyrenyl anion) can be ruled out based on theoretical predictions of a strong absorption feature in the 337–400 nm range (Hammonds & Sarre, private communication). It should be noted that the latter feature is at a higher energy than needed for electron detachment, so it may be that the pyrenyl anion does form but undergoes electron detachment before experiencing electronic excitation. While absorption from 2-aminopyrene and the pyrenyl anion could, in principle, overlap in wavelength with a pyrene absorption, the occurrence of this scenario is very improbable because the pyrene absorption feature retains its expected shape during photolysis. Smaller reactive species and products generated in the ammonia and water matrix must play a role, as both environments result in different final products. However, transitions associated with these remain undetected. For example, $NH_2$ has transitions throughout the visible region (Blindauer, Peric & Schurath 1993) and NH absorbs at 337 nm (Langford & Williamson 1998), but both species are not observed, not even in a pure ammonia ice. Both species are very likely present in the ice, but their low oscillator strengths (∼0.001–0.007) combined with line broadening due to matrix interactions likely prohibit a direct detection. For similar reasons, OH has not been observed in Ly$\alpha$-irradiated $H_2O$ ice (Bouwman et al. 2009).

## 4 DISCUSSION

### 4.1 $NH_3$ ice chemical process

While it is not possible to identify the reaction intermediates directly, the time (i.e. fluence) dependent behaviour of the PAH precursor and resulting anion can be monitored, providing additional insight into the processes induced by the UV radiation. The upper panel in Fig. 5 shows the integrated $B_{ghi}P$ and $B_{ghi}P^-$ absorbance during continuous vacuum UV irradiation of $B_{ghi}P$:$NH_3$ ice. The anion signal increases and reaches a maximum after about 2 min

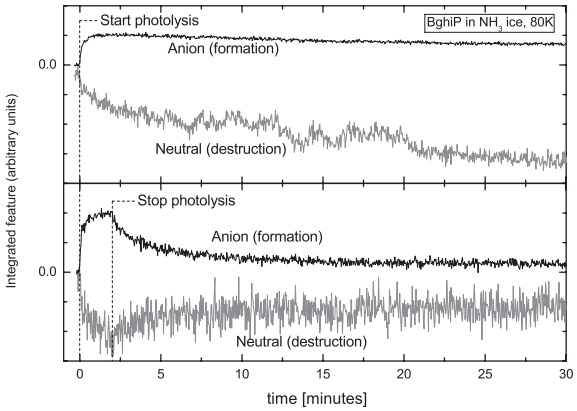


**Figure 5.** Integrated $B_{ghi}P$ absorbance in $NH_3$ ice upon vacuum UV irradiation as function of time (i.e. fluence). In the upper panel the ice is irradiated continuously for 2 h (only the first 30 min are shown). In the lower panel the vacuum UV irradiation is stopped after 2 min.

and then slowly decreases. In parallel, the neutral precursor is consumed during the whole irradiation process. In the lower panel of Fig. 5, the UV irradiation is stopped after 2 min. The anion signal decreases relatively quickly now and, simultaneously, the neutral PAH signal increases; it is likely that PAH anion is converted into PAH neutral via a charge–exchange type of reaction with an electron acceptor in the ice. The ongoing chemical processes are schematically summarized in an effective reaction scheme shown in Fig. 6. The focus here is on empirical trends and not on absolute numbers.

In this scheme, the PAH anion acts as a steady-state reaction product. When photolysis is halted, the $PAH^-$ peak disappears, as the $k_{12}$ reaction continues, converting the PAH anion back into its neutral form. Another $PAH^-$ destruction path, besides $e^-$ loss, may also occur during photolysis ($k_2$), given the fact that the $Py^-$ signal reaches a maximum and then decreases during ongoing irradiation. It is not possible to explicitly specify the resulting reaction products ($P_2$) because these are not visible in the spectral data (i.e. are not abundant enough to be observed, have low absorption strengths or absorb outside the accessible wavelength domain). Besides the conversion of PAH to $PAH^-$, the neutral PAH may also be destroyed through another photo-induced pathway, $k_1$, given the fact that in the ongoing irradiation experiment the neutral PAH signal decreases, even after the PAH anion formation signal stabilizes. Again, it is not possible to identify the products ($P_1$) of this pathway. Even the recent extension of the setup with a quadrupole mass spectrometer monitoring species desorbing from the ice during warm up has not helped. As a consequence, it cannot be excluded that $P_1$ is

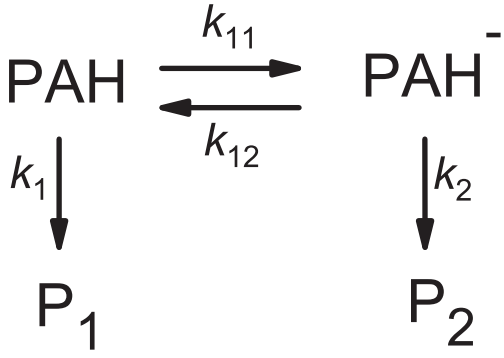


**Figure 6.** Effective reaction scheme for vacuum UV-irradiated PAH:$NH_3$ ice.

equivalent to $P_2$ and that the PAH anion is simply an intermediate in this conversion. Despite this lack of information on possible intermediates, it is likely that the $k_{11}$ reaction involves a direct electron transfer from ammonia photoproducts to the PAH neutral. The observed higher PAH anion production at increased temperatures signals that the $k_{11}$ reaction is enhanced when mobility of atoms or molecules in the ice is greater. Such a temperature effect is not a priori expected in a reaction involving the transfer of a free electron to a PAH molecule. The underlying reaction mechanism for $k_{11}$ involves a PAH and electron donating photofragment, suggesting a net scheme:

$$\mathrm{PAH} + \mathrm{NH_3} + \mathrm{H} \underset{\mathrm{UV}}{\longrightarrow} \mathrm{PAH^-} + \mathrm{NH_4^+},$$

where the hydrogen atom also originates from ammonia photolysis. It is probable that protonated ammonia, $NH_4^+$, forms as a counter ion to the PAH anion. IR studies have shown the formation of $NH_4^+$ in mixed ices containing ammonia. In ices that are exposed to vacuum UV photons, energetic electrons, high-energy protons or even simple heating, ammonia acts as a base and accepts a proton from an acid, creating $NH_4^+$ and a conjugate acid, as has been discussed for $OCN^-$ and $HCOO^-$ (Hudson, Moore & Gerakines 2001; Novozamsky, Schutte & Keane 2001; Bennett et al. 2010; Moon et al. 2010). In the IR, $NH_4^+$ has been observed in interstellar ices (Schutte & Khanna 2003). In the optical regime, $NH_4^+$ does not have absorption features. Complementary IR studies, therefore, are needed to further characterize the potential role of protonated ammonia in this reaction scheme.

Interestingly, while past studies showed ammonia-related ion formation in ices to be due to acid–base chemistry, the work presented here for PAHs reveals a different chemical process leading to the formation of PAH anions. These are found not to be produced by proton loss from the anion's parent molecule, as is the case for $OCN^-$ (Hudson et al. 2001). Rather, PAH anions form through simple electron acceptance from ammonia-related donor molecules. Since PAH electron affinities (EAs) increase with PAH size, with larger PAHs, it may be possible for this charge exchange to occur without energetic assistance.

### 4.2 Ammonia versus water ice

There is a clear difference between the behaviour of PAHs photolyzed in water versus ammonia ice. In $H_2O$ ice, pyrene, coronene, anthracene, benzo[ghi]perylene, naphthalene, quarterrylene and 4-methylpyrene are all converted to their monocationic or dicationic (for quaterylene) forms upon exposure to vacuum UV photons (Gudipati & Allamandola 2003, 2004, 2006b; Bouwman et al. 2009, 2010, 2011b). The $PAH^+$ molecules formed in water ice are highly stable and exist for days or longer, even after irradiation is stopped (Gudipati & Allamandola 2006a; Bouwman et al. 2009). In contrast, the $PAH^-$ molecules formed in ammonia ice convert back to their neutral form in the first few minutes after the photolysis has stopped (Fig. 5, lower panel). Unlike in ammonia ice, where ∼15 per cent of the consumed PAHs are converted to their anionic form, in water ice, 30–100 per cent of the consumed PAHs are converted to $PAH^+$ within ∼30 min of UV photolysis. Finally, during a long vacuum UV irradiation, $H_2O$:PAH ice undergoes complete conversion of the originally deposited PAHs, whereas in $NH_3$:PAH ice, only approximately 10 per cent of the originally deposited PAHs are consumed. The cause for this contrasting efficiency is not a priori clear but may be due to different wavelength-dependent absorption cross-sections of $NH_3$ with respect to $H_2O$ ice. Recently, it was shown that CO photodesorption depends on the wavelength of the impinging radiation (Fayolle et al. 2011). As stated before, the discharge lamp also emits light around 160 nm where water ice is essentially transparent (Mason et al. 2006), but ammonia ice is not. The difference in photoabsorption cross-section leads to different penetration depths of the vacuum UV photons in water versus ammonia ice. In ammonia ice, 99 per cent of the incident photons will be absorbed at a depth of 0.55 μm (calculated from Mason et al. 2006). This is consistent with the partial destruction of originally deposited PAHs.

Another cause of the different behaviour observed in water and ammonia PAH-containing ices lies in the energetics of charged molecule chemistry. The EAs of Py and $B_{ghi}P$ are 0.5 and 0.8 eV, respectively (Malloci et al. 2005), comparable to those of the ammonia photoproducts NH (EA = 0.38 eV; Al-Zaal, Miller & Farley 1987) and $NH_2$ (EA = 0.77 eV; Wickham-Jones et al. 1989). These EA values represent gas-phase calculations or measurements, but EA values in the solid phase can differ significantly, with changes of the order of 1–2 eV (Woon & Park 2004). The closeness between PAH, $NH_2$ and NH EA values means that PAHs in photolyzed $NH_3$ ice are near equal competitors for free electrons with the other ice components (NH and $NH_2$). This is not the case in water ice, where the photoproduct OH has an EA of 5 eV (Gudipati & Allamandola 2006a,b), making it a more favoured electron acceptor than PAH molecules. Water ice itself is also a possible electron acceptor, with a theoretical EA of 2–3 eV (Gudipati & Allamandola 2006a,b). The EA of ammonia ice has not been calculated or measured, but our results indicate that it is likely to be significantly smaller than that of water ice. Finally, experimental studies of electron transfer in solid ammonia and water at 20 K showed that water is much more effective at trapping electrons than ammonia (Lu & Sanche 2001). All these facts are consistent with a picture in which $H_2O$ ice converts PAHs more efficiently into $PAH^+$ than $NH_3$ ice into $PAH^-$, in full agreement with the experimental observations.

### 4.3 Astrophysical implications

$NH_3$ has been shown to be an important component of ices surrounding YSOs. In a *Spitzer* survey of 41 low-mass YSOs, Bottinelli et al. (2010) detected solid-phase $NH_3$ in roughly half of the survey sample, with abundances relative to water ranging from 2 to 15 per cent. Comparison of the $NH_3$ absorption maximum with laboratory spectra led Bottinelli et al. (2010) to conclude that ammonia is present in water-rich ice, as opposed to pure ammonia or $CO/CO_2$-rich ice. A Very Large Telescope/*Spitzer* study by Geers et al. (2009) of PAH emission features in 53 low-mass YSOs found a systematic lack of PAH spectral signatures in almost all the objects surveyed. Geers et al. (2009) concluded that these non-detections are most probably due to PAHs being frozen in ice layers, or in coagulated form, quenching the typical IR emission signatures. The results discussed here, particularly for highly diluted PAH abundances in $NH_3$:$H_2O$ 1:10 ice, are applicable to mixing rates observed in YSOs. The results indicate that under such conditions, PAH cations are likely to form. Following the experimental results found here for different water:ammonia mixtures, it is concluded that for a 10 per cent ammonia abundance with respect to water, the PAH chemistry likely will be dominated by cation formation schemes. The laboratory data presented here may also be of interest to Jupiter's upper atmosphere, where clouds of $NH_3$ ice particles have been observed (Brooke et al. 1998; Baines et al. 2002; Wong et al. 2004) and small PAHs have been studied as a condensation point for aromatic haze (Biennier et al. 2011). While the actual $NH_3$ clouds are only seen covering 1 per cent of the atmosphere, it is widely believed that the

clouds cover the entire atmosphere but are obscured from detection by a coating of haze. Atreya et al. (2005) proposed that the obscuring haze coating is comprised of PAHs. The atmosphere of Jupiter is exposed to solar UV photons, and conditions therefore may, in principle, be favourable for solid-state anion formation.

In summary, the experiments described here show that the ice environment is of fundamental importance and determines which solid-state reactions take place. The ice matrix constituents determine which solid-state reactions take place; the final charge may be positive or negative, depending on the relative amount of $NH_3$ to $H_2O$ in the ice. This effect has been specifically studied for PAHs but represents likely a more generally valid effect, also determining the spectral appearance of other interstellar ice constituents.

## ACKNOWLEDGMENTS

This research is financially supported by the Netherlands School for Astronomy, the Dutch Organization for Fundamental Research (FOM), NWO-VICI, the Dutch Organization for Science and the European Community's Seventh Framework Programme (FP7/2007-2013) under grant agreement no. 238258. EDT acknowledges support from an NWO Rubicon Fellowship. LJA gratefully acknowledges support from NASA's laboratory astrophysics and astrobiology programmes.

## REFERENCES

Al Zaal M., Miller H. C., Farley J. W., 1987, Phys. Rev. A, 35, 1099
Atreya S. K., Wong A. S., Baines K. H., Wong M. H., Owen T. C., 2005, Planet. Space Sci., 53, 498
Baines K. H., Carlson R. W., Kamp L. W., 2002, Icarus, 159, 74
Bennett C. J., Jones B., Knox E., Perry J., Kim Y. S., Kaiser R. I., 2010, ApJ, 723, 641
Bernstein M. P., Sandford S. A., Allamandola L. J., Gillette J. S., Clemett S. J., Zare R. N., 1999, Sci, 283, 1135
Bernstein M. P., Elsila J. E., Dworkin J. P., Sandford S. A., Allamandola L. J., Zare R. N., 2002, ApJ., 576, 1115
Bernstein M. P., Sandford S. A., Mattioda A. L., Allamandola L. J., 2007, ApJ, 664, 1264
Biennier L., Sabbah H., Chandrasekaran V., Klippenstein S. J., Sims I. R., Rowe B. R., 2011, A&A, 532, A40
Blindauer C., Peric M., Schurath U., 1993, J. Molecular Spectrosc., 158, 177
Bottinelli S. et al., 2010, ApJ., 718, 1100
Bouwman J., Paardekooper D. M., Cuppen H. M., Linnartz H., Allamandola L. J., 2009, ApJ, 700, 56
Bouwman J., Cuppen H. M., Bakker A., Allamandola L. J., Linnartz H., 2010, A&A, 511, 33
Bouwman J., Mattioda A. L., Linnartz H., Allamandola L. J., 2011a, A&A, 525, 93
Bouwman J., Cuppen S. M., Allamandola L. J., Linnartz H., 2011b, A&A, 529, 46
Brooke T. Y., Knacke R. F., Encrenaz Th., Drossart P., Crisp D., Feuchtgruber H., 1998, Icarus, 136, 1
Caro G. M. M. et al., 2002, Nat, 416, 403
Fayolle E. C., Bertin M., Romanzin C., Michaut X., Öberg K. I., Linnartz H., Fillion J. H., 2011, ApJ, 735, L36
Fuchs G. W., Cuppen H. M., Ioppolo S., Romanzin C., Bisschop S. E., Andersson S., van Dishoeck E. F., Linnartz H., 2009, A&A, 505, 629
Geers V. C., van Dishoeck E. F., Pontoppidan K. M., Lahuis F., Crapsi A., Dullemond C. P., Blake G. A., 2009, A&A, 495, 837
Gudipati M. S., Allamandola L. J., 2003, ApJ, 596, L195
Gudipati M. S., Allamandola L. J., 2004, ApJ, 615, L177
Gudipati M. S., Allamandola L. J., 2006a, ApJ, 638, 286
Gudipati M. S., Allamandola L. J., 2006b, J. Phys. Chem. A, 110, 9020
Guennoun Z., Aupetit C., Mascetti J., 2011, J. Phys. Chem. A, 115, 1844
Hudson R. L., Moore M. H., Gerakines P. A., 2001, ApJ, 550, 1140
Langford V. S., Williamson B. E., 1998, J. Phys. Chem. A, 102, 2415
Linnartz H. et al., 2011, in Cernicharo J., Bachiller R., eds, Proc. IAU Symp. 280, The Molecular Universe. Cambridge Univ. Press, Cambridge, p. 290
Lu Q. B., Sanche L., 2001, Phys. Rev. B, 63, 153403
Malloci G., Mulas G., Cappellini G., Fiorentini V., Porceddu I., 2005, A&A, 432, 585
Mason N. J. et al., 2006, Faraday Discuss., 133, 311
Moon E., Kang H., Oba Y., Watanabe N., Kouchi A., 2010, ApJ, 713, 906
Novozamsky J. H., Schutte W. A., Keane J. V., 2001, A&A, 379, 588
Öberg K. I., Garrod R. T., van Dishoeck E. F., Linnartz H., 2009, A&A, 504, 891
Öberg K. I., van Dishoeck E. F., Linnartz H., Andersson S., 2010, ApJ, 718, 832
Pontoppidan K. M., van Dishoeck E. F., Dartois E., 2004, A&A, 426, 925
Romanescu C., Marschall J., Kim D., Khatiwada A., Kalogerakis K. S., 2010, Icarus, 205, 695
Schutte W. A., Khanna R. K., 2003, A&A, 398, 1049
Shida T., 1988, Electronic Absorption Spectra of Radical Ions. Elsevier, Amsterdam
Šoustek P., Michl M., Almonasy N., Machalický O., Dvořák M., Lyčka A., 2008, Dyes Pigments, 78, 139
Tielens A. G. G. M., 2008, ARA&A, 46, 289
Wickham-Jones C. T., Ervin K. M., Ellison G. B., Lineberger W. C., 1989, J. Chem. Phys., 91, 2762
Wong M. H., Bjoraker G. L., Smith M. D., Flasar F. M., Nixon C. A., 2004, Planet. Space Sci., 52, 385
Woon D. E., Park J., 2004, ApJ, 607, 342

This paper has been typeset from a TEX/LATEX file prepared by the author.